



# Relating twin-tunnelling-induced settlement to changes in the stiffness of soil

Gang Zheng<sup>1</sup> · Ruikun Wang<sup>1</sup> · Huayang Lei<sup>1</sup> · Tianqi Zhang<sup>1</sup> · Jingzhuo Guo<sup>2</sup> · Zhuoran Zhou<sup>1</sup>

Received: 27 May 2021 / Accepted: 28 February 2022 / Published online: 25 March 2022  
© The Author(s), under exclusive licence to Springer-Verlag GmbH Germany, part of Springer Nature 2022

## Abstract

Recent research has shown that in a parallel twin-tunnel arrangement, the 2nd tunnel generates greater settlement than the 1st tunnel as the soil between the two tunnels softens. For other spatial twin-tunnel arrangements (twin tunnels with different cover depths), the pattern of settlement can be more complex and is inevitably affected by the order in which the two tunnels are constructed. Few studies have attempted to establish the relationship between the changes in soil stiffness and settlement behaviour. Hence, the settlement behaviour induced by twin tunnels is not yet well understood. A numerical model was created in this study, and a centrifuge model test was then used to verify the performance of this model. A series of comparative numerical analyses (e.g., inclined and overlapping twin tunnel arrangements) were performed to investigate the effect of the construction order and relative positions of the two tunnels. The relationship between the changes in soil stiffness and settlement behaviour was well established. The mechanisms by which the 1st tunnel affects the settlement behaviour produced by the 2nd tunnel were clarified.

**Keywords** Changes in the stiffness · Different cover depths · Sequential construction of twin tunnels · Settlement behaviour

## List of symbols

$E_p$	Young's modulus of the lining in the isotropic plane
$E_n$	Young's modulus of the lining in normal direction of the isotropic plane
$\nu_p$	Poisson's ratio of the lining
$G_n$	Shear modulus of the lining
$M$	Critical state friction coefficient
$\lambda^*$	Gradient of the normal compression line in $\ln v$ - $\ln p'$ space
$\kappa^*$	Gradient of the elastic swelling line in $\ln v$ - $\ln p'$ space
$e_{cs}$	Void ratio of isotropically normally compressed soil when $p' = 1$ kPa
$A$	Elastic shear modulus used in the 3-SKH model
$T$	Ratio of the size of the history surface to the bonding surface
$S$	Ratio of the size of the yield surface to the history surface
$\psi$	Exponent in the hardening modulus

## 1 Introduction

Tunnels are often constructed in major cities worldwide to account for the pressing demand for more convenient and efficient traffic facilities. The surface settlement trough induced by a single tunnel can be effectively predicted by a Gaussian curve [7, 22, 26, 27]. However, single tunnel construction is rarely adopted in practice. To allow bi-directional traffic, twin tunnels are one of the most common forms of traffic flow in urban underground design. Twin tunnels are often constructed separately and excavated in a sequential manner.

A superposition method proposed by O'Reilly & New [25] has been extensively adopted to predict surface settlement troughs induced by twin tunnels. The superposition method was defined as a direct combination of multiple settlement troughs induced by the individual tunnels excavated in the greenfield site. This method did not consider the interaction between the two tunnels (the interaction mainly considered the influence of the 1st tunnel on the settlement behaviour induced by the 2nd tunnel), which

✉ Tianqi Zhang  
TianqiZhang@tju.edu.cn

<sup>1</sup> School of Civil Engineering, Tianjin University, Tianjin 300072, China

<sup>2</sup> China State Construction Engineering Corporation, Beijing, China

could result in an underestimation of the magnitude of the settlement. In situ observations have shown that, compared with the 1st tunnel, the 2nd tunnel can result in greater surface settlement [8, 9, 24]. Substantial construction risks and potential safety hazards may be encountered during twin tunnelling. Therefore, it is necessary to investigate the influence of the 1st tunnel on the soil settlement induced by the 2nd tunnel.

Yamaguchi et al., Addenbrooke and Potts, Hunt et al. [1, 3, 15, 32] carried out a series of finite element analyses to simulate twin tunnel construction. Chu et al., Kim et al., Chapman et al., Suwansawat & Einstein, Chen et al., Kirsch, Idinger et al., He et al., Divall and Goodey, Chen et al., Liu et al., and Ma et al. [2, 4–6, 11, 12, 14, 16–21, 30] performed a number of physical model tests to analyse the settlement behaviour of soil. Many scholars have uncovered the settlement regularities induced by twin tunnels. However, the mechanisms behind such soil settlement behaviour are not well understood.

Divall et al. [13] analysed the variations in the shear stiffness around two tunnels using the surface and subsurface settlements obtained from a series of centrifuge tests and found that the influence of the 1st tunnel on the soil settlement induced by the 2nd tunnel can be inferred by the changes in soil stiffness. By performing numerical modelling, Zhang et al. [33] successfully illustrated the settlement behaviour induced by two parallel tunnels based on the changes in soil stiffness around the 2nd tunnel. The results indicated that the soil between the two tunnels softened due to the excavation of the 1st tunnel. More surface settlement was generated, and thus, the settlement trough became deeper. However, the parallel arrangement is only one special case where two tunnels are symmetrical and have the same cover depths. Many twin tunnels have been excavated in other spatial arrangements (e.g., inclined and overlapping arrangements). The settlements induced by twin tunnels with different cover depths differ greatly from those induced by tunnels arranged in parallel. For instance, in the overlapping arrangement, the final accumulated settlements were lower than those induced by two single tunnels in a greenfield, and thus, the settlements were overestimated by the superposition method [1]. In addition, the settlements induced by twin tunnels with different cover depths can be more complex and inevitably affected by the construction order. However, little research has been conducted on general spatial twin tunnel arrangements to establish the relationship between twin-tunnelling-induced settlements and changes in soil stiffness. The mechanisms behind such settlement behaviour are not well understood.

In this study, numerical analyses were carried out to study the settlement behaviour of soil in general spatial twin tunnel arrangements based on the changes in soil

stiffness. First, a centrifuge model test performed by Divall [10] was adopted, and the experimental process was carefully replicated to verify the performance of the model. Various arrangements of twin tunnels with different cover depths (e.g., inclined and overlapping arrangements) were simulated at the prototype scale using the stress release method, and the effect of the construction order and relative position of the twin tunnel was analysed. The maximum settlement ( $S_{\max}$ ) and settlement trough width ( $i$ ) of the resulting surface and subsurface settlement troughs were analysed in detail. The soil settlement behaviour was further analysed based on the changes in soil stiffness around the 2nd tunnel. The soil settlement behaviour and its interaction mechanisms for the sequential construction of twin tunnels were finally clarified.

## 2 Establishment of the numerical model

### 2.1 Modelling approach

In this paper, twin tunnel construction was modelled using the stress release method. This method has been validated as an effective method for modelling tunnel construction in a two-dimensional configuration [1, 3, 15]. The simulation was performed at full scale and the process included a total of 7 steps:

- a) *Initial state ( $K_0$  consolidation)* The model was initialized by a normally consolidated state. The stress condition,  $K_0 = 1 - \sin \varphi$ , was adopted to achieve  $K_0$  consolidation in the solid–fluid coupling mode in a greenfield. The tunnel lining was assumed to be impermeable. The boundary condition of the pore pressure at both sides of the model was set to linearly increase with depth, exhibiting a triangular distribution (cf. Figure 1a).
- b) *Excavation of the 1st tunnel* The 1st tunnel was excavated by removing the corresponding elements at the very beginning of this step. The overall displacements of all the nodes around the tunnel were constrained afterwards. The nodal reaction forces acquired at the fixed tunnel boundary could be taken as the initial support pressure for support (cf. Figure 1b).
- c) *1st tunnelling event* The tunnel boundary was freed, and the initial support forces were applied to all nodes around the 1st tunnel, which corresponds to the constraint condition of the 1st tunnel at the end of step (b). To model the tunnel excavation, a ‘time-dependent stress release’ method was adopted. The initial support pressure was linearly reduced over the step time. The reduction in support pressure was

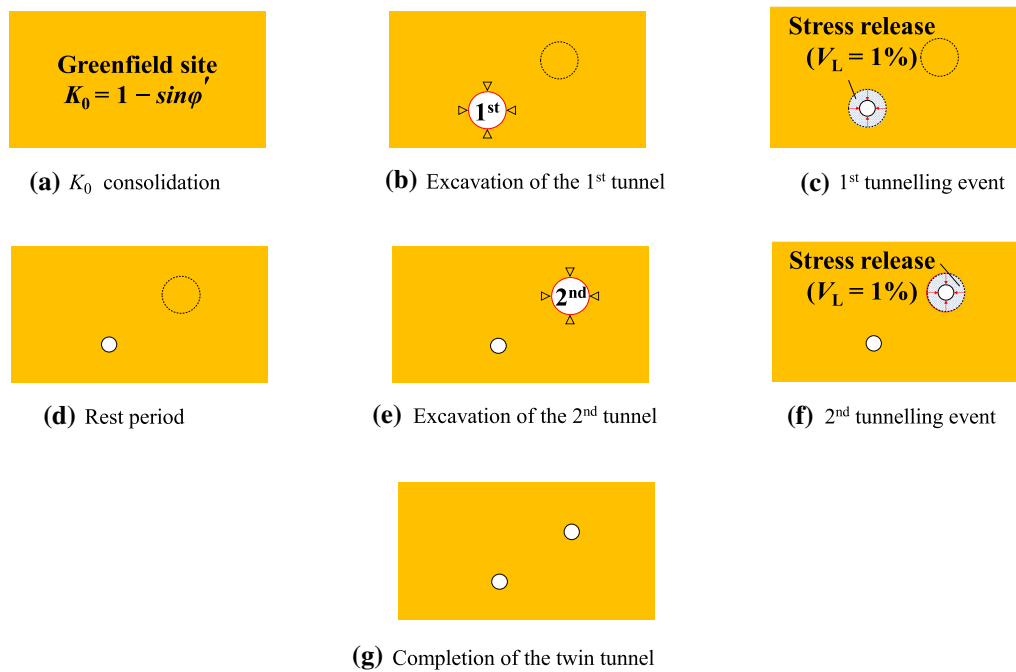


Fig. 1 Simulation procedure for twin tunnel construction

determined by measuring the volumetric change of the tunnel using a script coded in Python (the Python code and relevant instructions are given in the supplemental material). The duration for the excavation of the 1st tunnel was 7 days. The tunnel lining, which was made of C50 concrete with an elastic modulus ( $E_{ela}$ ) of 34.5 GPa, a thickness of 0.3 m and a bulk density of 25 kN/m<sup>3</sup>, was implemented immediately upon the excavation. The thickness of 0.3 m was adopted in both the practical engineering and the numerical model. The tunnel lining was modelled using shell elements and a transversely isotropic model [34]. The lining parameters are given in Table 1. These parameters are explained in the list of notations below. (cf. Figure 1c).

- d) *Rest period* A rest period of 21 days was allowed immediately after the completion of the 1st tunnel, which represented a construction delay before the 2nd tunnelling event for the soil mass to consolidate and settle without any disturbance (cf. Figure 1d).
- e) *Excavation of the 2nd tunnel* The operations performed for the 1st tunnel in step (b) were repeated for the 2nd tunnel (cf. Figure 1e).

- f) *2nd tunnelling event* The operations performed for the 1st tunnel in step (c) were repeated for the 2nd tunnel (cf. Figure 1f).
- g) *Completion of the twin tunnel* Twin tunnel construction was complete when the volume loss for each tunnel reached 1%, followed by sufficient time for soil movements to develop (cf. Figure 1e).

### 2.2 Constitutive model

The three-surface kinematic hardening (3-SKH) model was adopted as the constitutive model in the numerical simulation (Fig. 2). This constitutive model was an extension of the Modified Cam-Clay (MCC) model. Two additional surfaces (yield surface, YS; history surface, HS) were introduced within the MCC critical state bonding surface

Table 1 Tunnel lining parameters

$E_{ela}$ (kPa)	$E_p$ (kPa)	$E_n$ (kPa)	$\nu_p$	$G_n$ (kPa)
34,500,000	25,875,000	34,500,000	0.2	10,781,250

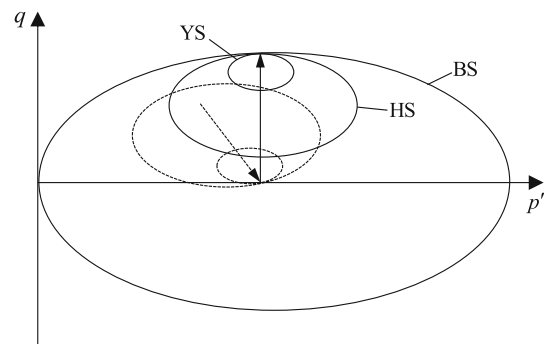


Fig. 2 Sketch of 3-SKH model in  $p'$ - $q$  plane

(BS). If a stress point  $(p', q)$  in  $p'$ - $q$  space is within the YS surface, soil displays elastic deformation and high small-strain stiffness, which is formulated in Eq. 1. When the stress point is in contact with the YS surface (cf. Eq. 2), soil starts to enter the yield state and then the YS surface translates along the subsequent stress path direction. In addition, if a stress reversal is detected, such a translation rule allows the stress point to return to the YS surface and has the merit of reintroducing the high stiffness of soil. As the stress path extends, the stress point is in contact with the HS surface which is defined by Eq. 3. The YS surface also intersects with the HS surface at the current stress point. The translation rule of the HS surface is the same as that of the YS surface. Finally, when the stress point and all the surfaces (YS, HS, and BS surfaces) are in contact, the 3-SKH model reduces to the MCC model and the soil reaches the failure state on the critical state line (the equation of the bonding surface is given in Eq. 4). In this way, the effect of recent stress history on the soil behaviour could be simulated using the 3-SKH model.

$$\begin{bmatrix} \delta \varepsilon_v^e \\ \delta \varepsilon_s^e \end{bmatrix} = \begin{bmatrix} \kappa^*/p' & 0 \\ 0 & 1/3G'_{ec} \end{bmatrix} \begin{bmatrix} \delta p' \\ \delta q \end{bmatrix} \quad (1)$$

$$(p' - p'_b)^2 + \frac{(q - q_b)^2}{M^2} = T^2 S^2 p_0'^2 \quad (2)$$

$$(p' - p'_a)^2 + \frac{(q - q_a)^2}{M^2} = T^2 p_0'^2 \quad (3)$$

$$(p' - p_0')^2 + \frac{q^2}{M^2} = p_0'^2 \quad (4)$$

where  $p'$  and  $q$  refer to the current stress state.  $p_0'$  refers to the centre of the bonding surface.  $p'_a$  and  $q_a$  refer to the centre of the history surface.  $p'_b$  and  $q_b$  refer to the centre of the yield surface.  $G'_{ec}$  refers to the elastic shear modulus of soil at small strain.  $\varepsilon_v^e$  and  $\varepsilon_s^e$  refer to the elastic volumetric and shear strain, respectively.

According to Stallebrass and Taylor [29], the previous stress path before the current stress changes, which affected the stiffness of the soil, was termed the recent stress history. The changes in the stiffness of the soil would accordingly affect the soil behaviour. In this way, this model can consider the effect of the stress history on soil stiffness in a multistage simulation, by which the effect of soil disturbance around the 1st tunnel on the soil stiffness and ground settlement behaviour of the 2nd tunnel could be effectively simulated.

Numerical analyses were carried out using the commercial finite element software ABAQUS (version 2016). The 3-SKH model was implemented using a user-defined material subroutine (UMAT), which was reprogrammed in FORTRAN, following the original version used in CRISP

by Stallebrass [28] and the C++ version used in TOCHNOG by Masin [23].

A centrifuge model test was selected for the validation of the 3-SKH model. A schematic diagram of the physical and numerical model is shown in Fig. 3. More details of the centrifuge model test and corresponding numerical simulation can be found in the Appendix. Speswhite kaolin clay was adopted in this test. The soil parameters for the 3-SKH model have been well documented in many collaborative studies by researchers at City University of London [28, 31], as shown in Table 2. In Table 2,  $M$ ,  $\lambda^*$ ,  $\kappa^*$ ,  $e_{cs}$ , and  $A$  were five parameters in the MCC model.  $T$ ,  $S$ , and  $\psi$  were three exclusive parameters in the 3-SKH model. These parameters are explained in the list of notations below.

The comparison between the measured and computed data is shown in Fig. 4. The surface settlement troughs obtained by the numerical simulation were basically analogous to those of the test data. Both the numerical simulation and the centrifuge model test showed that the 2nd tunnelling event produced deeper and narrower settlement troughs than the 1st tunnelling event (for the experimental data and numerical results, the  $S_{max}$  induced by the 2nd tunnel was approximately 25% and 28% greater than that induced by the 1st tunnel, respectively, and the  $i$  induced by the 2nd tunnel was approximately 5% and 6% lower than that induced by the 1st tunnel, respectively). As a consequence, the 3-SKH model could effectively model the excavation of twin tunnels.

### 3 Simulated cases

Five cases, namely, N1–N5, were considered in this paper and are summarized in Table 3. Unlike the above-mentioned numerical simulation, these five cases were performed at the prototype scale. A schematic diagram of the two-dimensional plain-strain model is shown in Fig. 5. Each tunnel had a diameter ( $D$ ) of 6.6 m. The upper tunnel had a cover depth ( $C$ ) of  $2D$ . The vertical and lateral extents of the model were maintained at  $3D$  and  $6D$ , respectively, to eliminate possible boundary effects. Various twin tunnel arrangements (parallel, inclined and overlapping arrangements) were modelled with a centre-to-centre spacing ( $S$ ) of  $1.5D$ . The centre of the 1st tunnel and positive  $x$ -axis were assumed to be the origin and polar axis, respectively, in the polar coordinate system. For a better understanding, in Table 3, the angle ( $\theta$ ) of the 2nd tunnel with respect to the polar axis was proposed to represent the relative positions of twin tunnel. The time allowed for the construction of each tunnel was set to 7 days. The  $V_t$  of each tunnel was set to 1% based on the

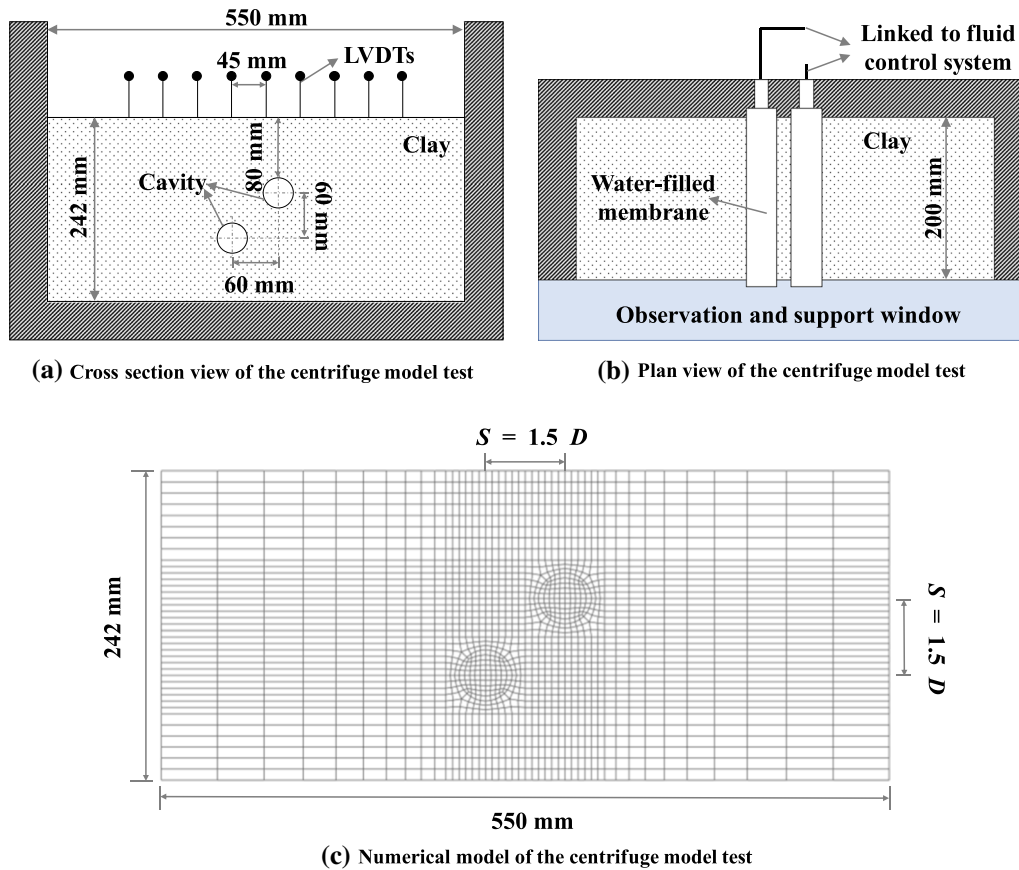


Fig. 3 Schematic diagram of the centrifuge model

Table 2 Soil parameters for the 3-SKH model

$M$	$\lambda^*$	$\kappa^*$	$e_{cs}$	$A$ (kPa)	$T$	$S$	$\psi$	$k_v$ (mm/s)	$k_h$ (mm/s)
0.89	0.073	0.005	1.994	1964	0.25	0.08	2.5	$4.7 \times 10^{-7}$	$1.37 \times 10^{-6}$

stress release method. A delay of 21 days between the construction of the two tunnels was used in the simulation and considered the rest period.

## 4 Results

### 4.1 Surface settlement induced by the 1st tunnel

The maximum net surface settlement and trough width induced by the 1st tunnel were labelled  $S_{max1}$  and  $i_1$ , respectively. The settlement trough was symmetrical about the centreline of the 1st tunnel as the tunnel was excavated in a greenfield site (cf. Figure 6). The shallower the tunnel cover is, the deeper and narrower are the surface settlement trough.

### 4.2 Final accumulated surface settlement induced by twin tunnelling

The final accumulated surface settlement, ( $S_{max}$ ), induced by twin tunnelling is given in Fig. 7. The superposition of  $S_{max}$  induced by each tunnel at the positions of the two tunnels is also shown in Fig. 7. The superposition method neglects the twin-tunnel interaction and severely underestimates the  $S_{max}$  induced by twin tunnelling. When the two tunnels were excavated in a parallel arrangement,  $S_{max}$  was 58% greater than that of the superposition method. For the inclined arrangements N2 and N3, the  $S_{max}$  values were 35% and 44% greater than those of the superposition method, respectively. The excavation of the overlapping twin-tunnel arrangements N4 and N5 exhibited obvious differences in  $S_{max}$ , and the values were 27% and 59%



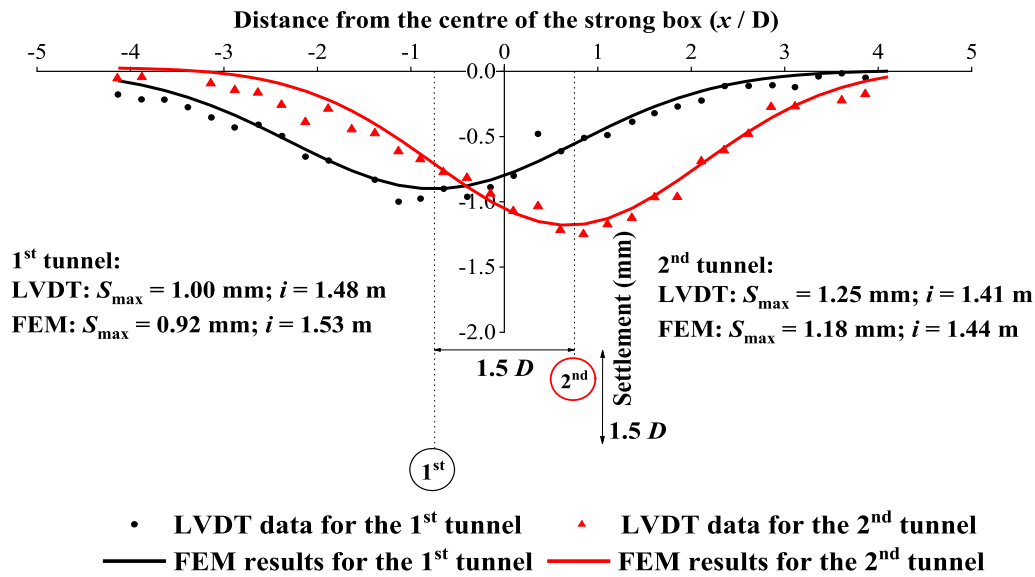


Fig. 4 Comparisons of the computed and measured surface settlements

Table 3 Details of the twin tunnel numerical simulation series

Test ID	Relative positions	1st tunnel	Angle (°)	Cover depth ratio (C/D)	Space ratio (S/D)
N1	Parallel	Left	0	2	1.5
N2	Inclined	Upper	-135	2 and 3.06	1.5
N3	Inclined	Lower	45	2 and 3.06	1.5
N4	Overlapping	Upper	-90	2 and 3.5	1.5
N5	Overlapping	Lower	90	2 and 3.5	1.5

greater than those of the superposition method. Therefore, the effect of the disturbance of the 1st tunnel on soil deformation behaviour needs to be further investigated.

As shown in Fig. 7,  $S_{max}$  was independent of the construction order for the symmetrical configuration of the parallel twin tunnel. However, the construction order can have great implications for twin-tunnel surface settlement depending on cover depth (e.g., inclined and overlapping arrangements). When the upper tunnel was excavated second,  $S_{max}$  was 6% and 25% greater than that induced when the lower tunnel was excavated second in the inclined and overlapping arrangements, respectively.

### 4.3 Net surface settlement induced by the 2nd tunnel

The maximum net surface settlement and trough width induced by the 2nd tunnel were labelled  $S_{max2}$  and  $i_2$ , respectively. If the twin tunnel was excavated in a parallel arrangement (the angle  $\theta$  is  $0^\circ$  in N1), the settlement trough

induced by the 2nd tunnel was independent of the construction order, as the two tunnels were symmetrical and had the same cover depth. As shown in Fig. 8a, compared to the values induced by a single tunnel at the position of the 2nd tunnel,  $S_{max2}$  was 32% greater than  $S_{max1}$ , while  $i_2$  was 9% lower. These results seem to match the results obtained by Zhang et al. [33]. However, for twin tunnels with different cover depths and relative positions, the variation trend of  $S_{max2}$  and  $i_2$  can be quite complex.

When the upper tunnel was excavated first (the angle  $\theta$  was  $-135^\circ$  in N2 and  $-90^\circ$  in N4),  $i_2$  was substantially affected by the presence of the 1st tunnel, and  $i_2$  was 46% and 59% greater than that induced by a single tunnel at the position of the 2nd tunnel. However,  $S_{max2}$  was not substantially affected by the 1st tunnel, and  $S_{max2}$  was 9% and 17% lower than that induced by a single tunnel (cf. Fig. 8b, d).

When the lower tunnel was excavated first (the angle  $\theta$  is  $45^\circ$  in N3 and  $90^\circ$  in N5),  $S_{max2}$  was found to be substantially affected by the presence of the 1st tunnel.  $S_{max2}$  was 26% and 61% greater than that induced by a single tunnel at the position of the 2nd tunnel. However,  $i_2$  was not substantially affected by the 1st tunnel.  $i_2$  was 1% and 22% lower than that induced by a single tunnel (cf. Fig. 8c, e).

In conclusion, if the 2nd tunnel is a shallowly buried tunnel,  $S_{max2}$  may experience a stronger disturbance than  $i_2$ ; otherwise,  $i_2$  may experience a greater disturbance than  $S_{max2}$ .

To gain further insight into the interaction mechanism between twin tunnels, the subsurface deformation responses are also given in Figs. 9 and 10 for  $S_{max2}$  and  $i_2$ , respectively. In comparison with single-tunnelling-induced

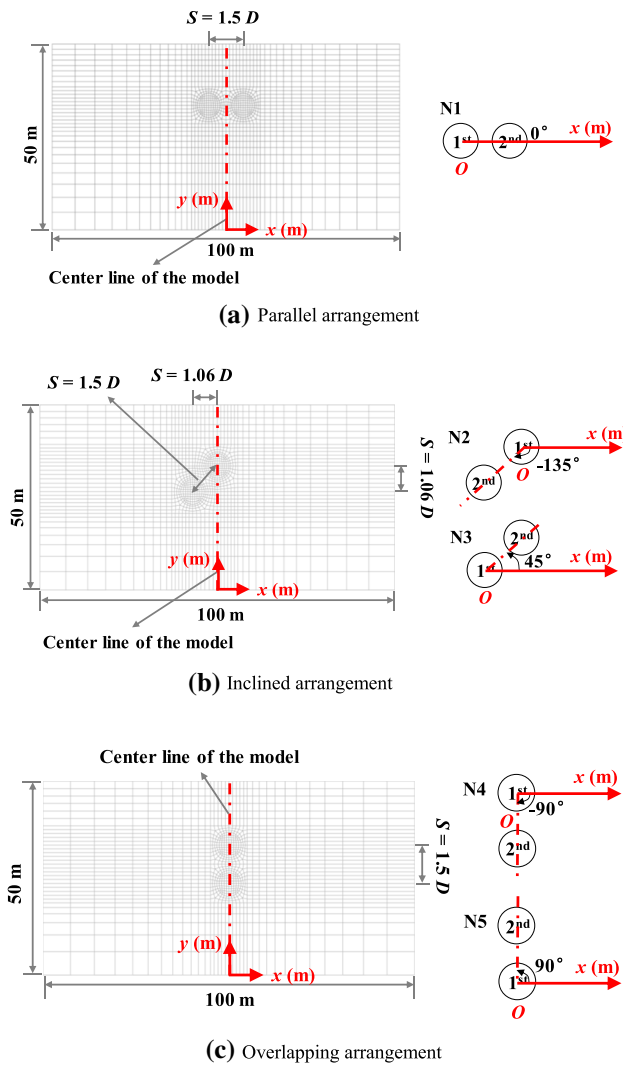


Fig. 5 Schematic diagram of the twin tunnel numerical model

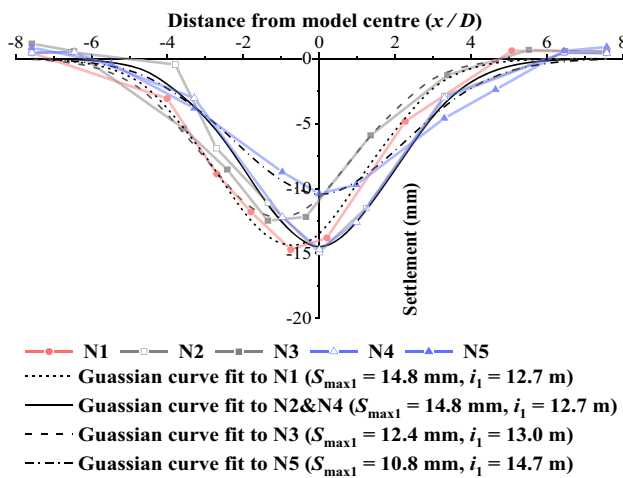


Fig. 6 Surface settlement induced by the 1st tunnel

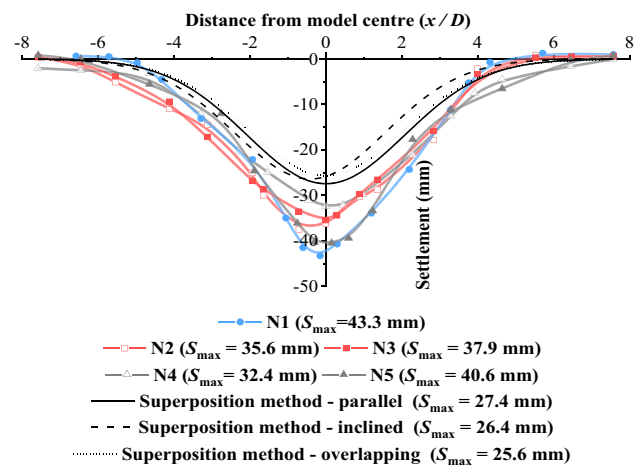


Fig. 7 Final accumulated surface settlements induced by twin tunnelling

subsurface settlement, the variations in  $S_{max2}$  were opposite to those in  $i_2$ . Figure 9 shows that the  $S_{max2}$  induced by N3 and N5 was considerably greater than that induced by a single tunnel at the same position as the 2nd tunnel. In contrast,  $S_{max2}$  induced by N2 and N4 was slightly lower than that induced by the single tunnelling event.

As shown in Fig. 10,  $i_2$  induced by N3 and N5 was slightly lower than that induced by a single tunnel at the same position of the 2nd tunnel. However,  $i_2$  induced by N2 and N4 was much greater than that induced by the single tunnelling event. The results measured deep underground were consistent with those at the surface, and the surface and subsurface settlement behaviour could be attributed to the displacement patterns surrounding the 2nd tunnel [33].

#### 4.4 Explanation of the soil deformation behaviour during twin tunnelling

To explain the abovementioned observations, additional settlements were defined in this section and were calculated by subtracting the net soil settlements induced by the 2nd tunnel from those induced by a single tunnel at the position of the 2nd tunnel. If the soil settlements induced by the 2nd tunnel were greater than those induced by a single tunnel, the additional settlements were assumed to be positive. In this way, the distribution of the main additional settlements surrounding the 2nd tunnel parallel to the 1st tunnel is given in Fig. 11. In the parallel arrangement, the angle  $\theta$  is  $0^\circ$  in N1, and the soil between the two tunnels settled more than that at other locations, which represented positive additional settlement relative to that of a single tunnelling event. In contrast, the soil at the crown region of the 2nd tunnel experienced less settlement, which represented negative additional settlement. Hence, the settlement

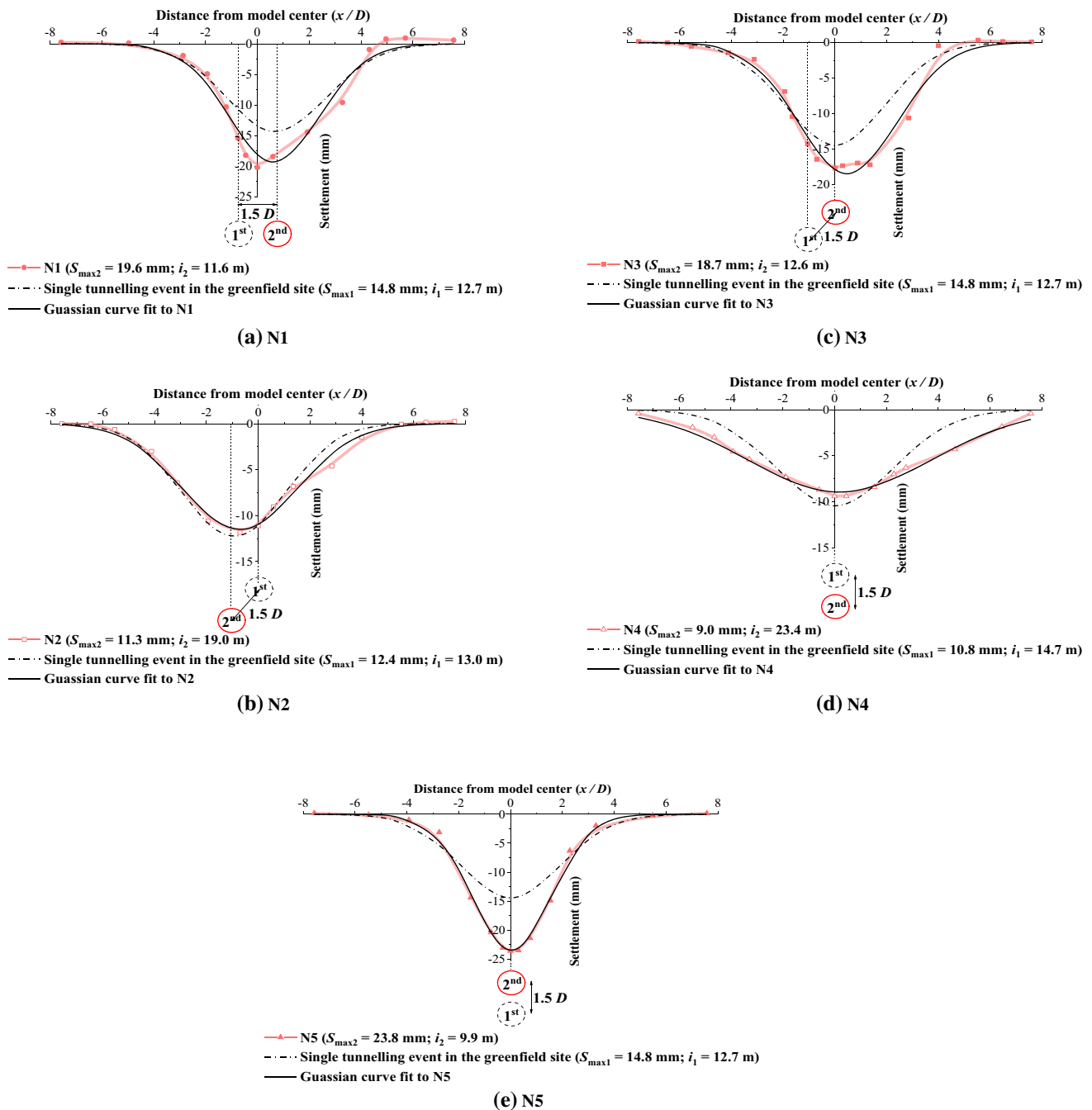


Fig. 8 Net surface settlement induced by the 2nd tunnel

trough induced by the 2nd tunnel was deeper and narrower than that induced by the 1st tunnel.  $S_{max2}$  was greater due to the positive additional settlement between the two tunnels. In fact, the variations in the settlement trough can be effectively explained by the soil displacement surrounding the 2nd tunnel. More inward displacements occurred at the shoulder and springline of the 2nd tunnel, while fewer inward displacements occurred at the crown of the 2nd tunnel. This displacement pattern was attributed to the

changes in the soil stiffness around the 2nd tunnel [33]. In this study, the secant shear modulus ( $G_s$ ) was defined to represent the soil stiffness, which can be expressed as:

$$G_s = \left| \frac{\Delta q}{\Delta \epsilon_s} \right| \tag{5}$$

where the deviatoric stress  $q$  and shear strain  $\epsilon_s$  can be defined as:



$$q = \sqrt{\frac{1}{2} \left[ (\sigma_x - \sigma_y)^2 + (\sigma_x - \sigma_z)^2 + (\sigma_y - \sigma_z)^2 + 6(\tau_{xy}^2 + \tau_{xz}^2 + \tau_{yz}^2) \right]} \tag{6}$$

$$\varepsilon_s = \sqrt{\frac{2}{9} \left[ (\varepsilon_x - \varepsilon_y)^2 + (\varepsilon_x - \varepsilon_z)^2 + (\varepsilon_y - \varepsilon_z)^2 + 6(\varepsilon_{xy}^2 + \varepsilon_{xz}^2 + \varepsilon_{yz}^2) \right]} \tag{7}$$

The ratio  $G_{s1}/G_{s0}$  was adopted to show the changes in soil stiffness under the influence of the 1st tunnel.  $G_{s1}$  represents the soil stiffness around the 2nd tunnel during its construction.  $G_{s0}$  represents the soil stiffness induced by a single tunnel at the same position as the 2nd tunnel in the greenfield site. A ratio value ( $G_{s1}/G_{s0}$ ) of less than 1.0 indicated that the soil softened; otherwise, the soil hardened. The variations in the soil stiffness around the 2nd tunnel are given in Fig. 11. The soil at the springline region of the 2nd tunnel softened, and thus, more inward displacements were generated. The soil at the crown region of the 2nd tunnel hardened, and fewer inward displacements were generated.

For twin tunnels with different cover depths and relative positions, the variations in the settlement troughs induced by the 2nd tunnel can also be explained based on the changes in soil stiffness.

When the upper tunnel was excavated first (the angle  $\theta$  is  $-135^\circ$  in N2 and  $-90^\circ$  in N4), the soil at the shoulder and springline region of the 2nd tunnel softened. Therefore, the soil in these regions was displaced towards the 2nd tunnel, and positive additional settlements were generated

accordingly. In addition, the soil at the crown region of the 2nd tunnel hardened, and less inward displacement occurred above the crown region of the 2nd tunnel than for a single tunnel, resulting in a lower  $S_{max2}$ . The surface settlement trough became increasingly shallow and broad, and  $i_2$  was considerably greater than that induced by a single tunnel (cf. Fig. 13a, b).

When the lower tunnel was excavated first (the angle  $\theta$  is  $45^\circ$  in N3 and  $90^\circ$  in N5), the soil at the shoulder and springline region to both sides of the 2nd tunnel softened and was displaced towards the 2nd tunnel to a greater degree. Due to the softening effect, positive additional settlement was generated on both sides of the 2nd tunnel and finally extended upwards to the surface, leading to greater value of  $S_{max2}$ , whereas  $i_2$  was lower than that induced by a single tunnel as the surface settlement trough became deeper (cf. Fig. 12a, b).

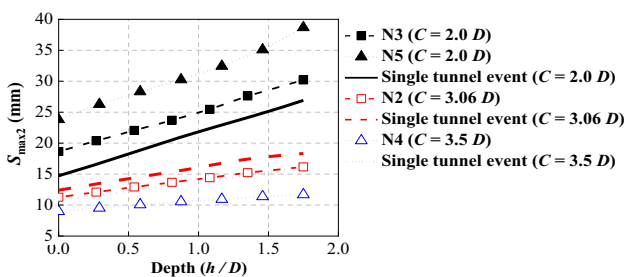


Fig. 9 Variations in  $S_{max2}$  with increasing depth

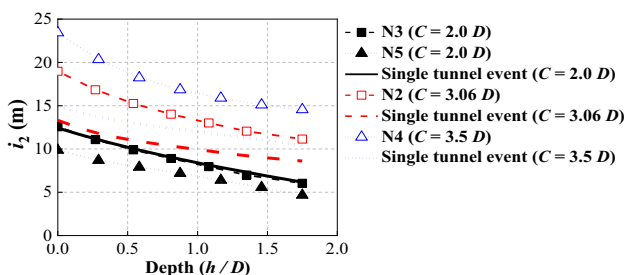


Fig. 10 Variations in  $i_2$  with increasing depth

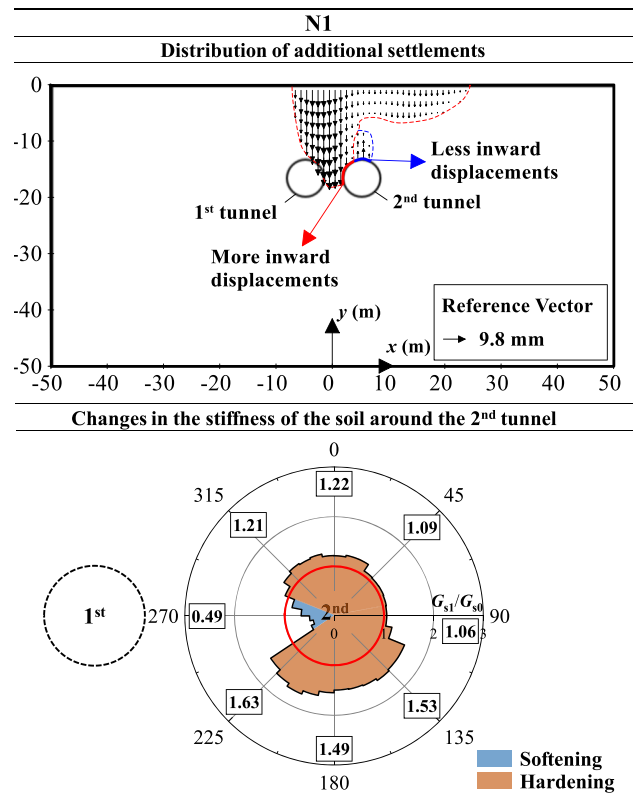


Fig. 11 Distribution of additional settlements and changes in the soil stiffness around the 2nd tunnel (parallel arrangement)

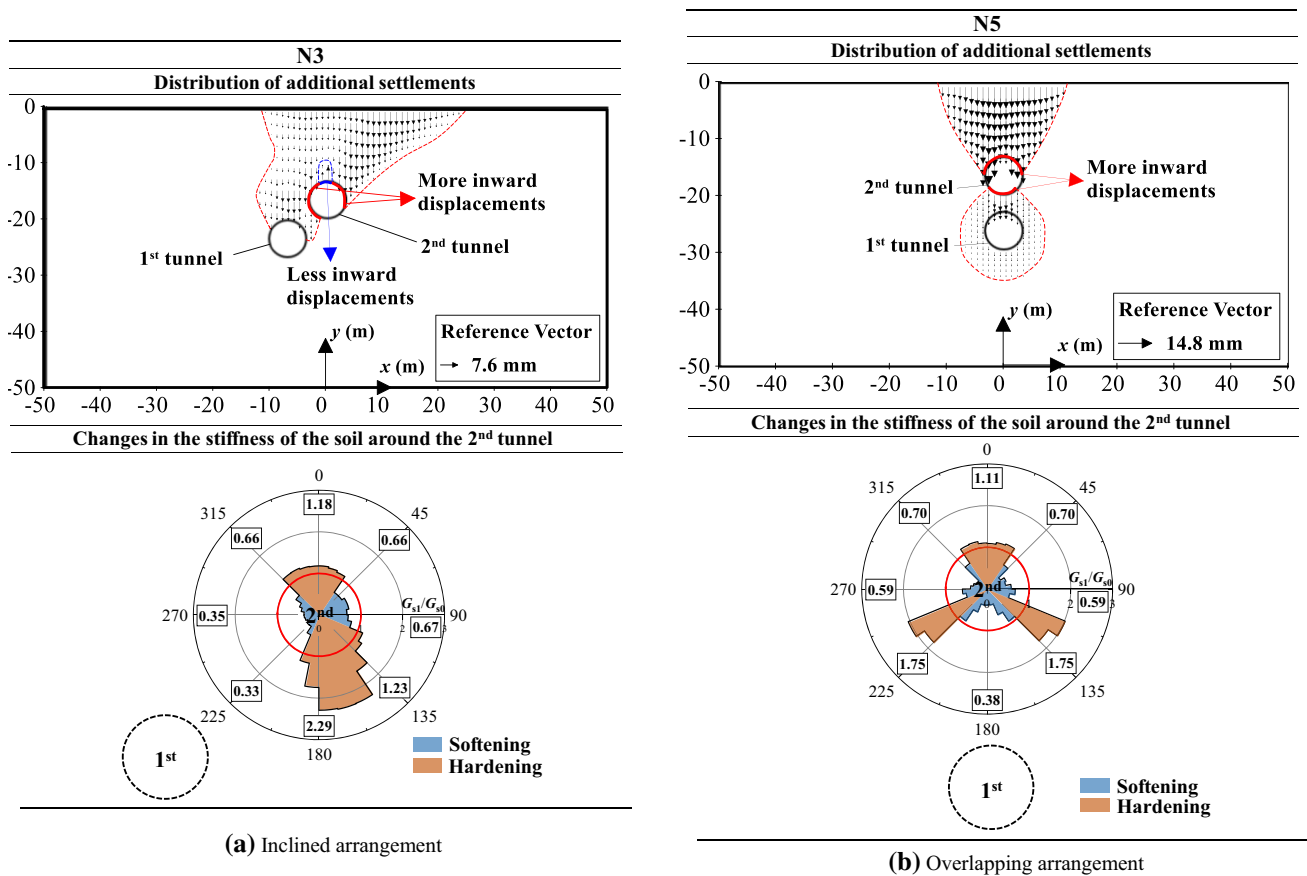


Fig. 12 Distribution of additional settlements and changes in the soil stiffness around the 2nd tunnel (the upper tunnel was excavated second)

It was also found that the soil at the invert region of the 2nd tunnel hardened, except when the 2nd tunnel was excavated right above the lower tunnel in the overlapping arrangement (the angle  $\theta$  is  $90^\circ$  in N5). Nevertheless, no obvious additional settlements were observed at the tunnel invert, although the soil hardened or softened there (cf. Figs. 11, 12a, 13). Basically, this hardening or softening effect on soil at the invert region has little impact on the convergence of the 2nd tunnel and the ground settlement. In other words, the effect of the 1st tunnel event on soil at the invert region of the 2nd tunnel was not strong enough to lead to the changes in surface settlements.

### 5 Conclusions

This article focuses on the investigation of the surface settlement trough induced by twin tunnels with different cover depths. The effect of the order in which the two tunnels were constructed was analysed as well. The following conclusions could be drawn for the tunnelling conditions considered in this study.

1. If the lower tunnel was excavated first, the soil at the shoulder and springline regions of the 2nd tunnel softened. The resulting inward displacements induced positive additional settlements at the surface, which resulted in a higher  $S_{max2}$  than produced by a single tunnel. The surface settlement trough became deeper so  $i_2$  was deemed to be lower.
2. If the upper tunnel was excavated first, the soil at the shoulder and springline regions closer to the 1st tunnel softened. In addition, the soil at the crown region hardened. Due to the changes in soil stiffness, more inward displacements were generated at the shoulder and springline regions closer to the 1st tunnel, while fewer inward displacements were generated at the crown region. Therefore, positive additional settlement occurred between the two tunnels, while negative additional settlement occurred above the crown region of the 2nd tunnel. As the tunnels were excavated, the surface settlement trough became increasingly shallow and broad,  $S_{max2}$  was lower, and  $i_2$  was greater.

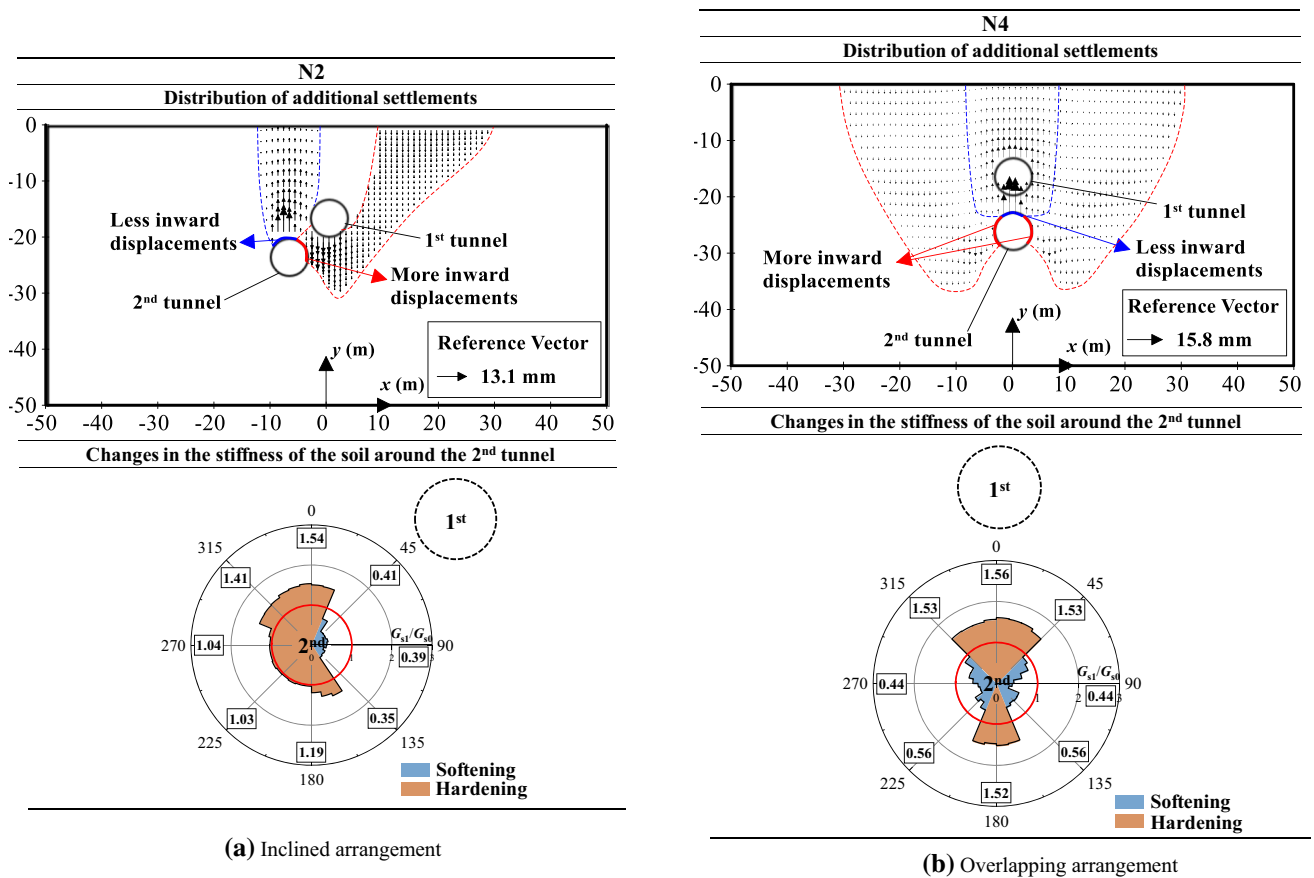


Fig. 13 Distribution of the additional settlements and changes in the soil stiffness around the 2nd tunnel (the lower tunnel was excavated second)

## Appendix: Numerical simulation for the centrifuge model test

### Centrifuge model test

The centrifuge model test simulated in this study was performed by Divall [10] at City University of London. The model was 550 mm wide, 242 mm high and 200 mm thick. The two cavities inside the strong box had the same diameter ( $D$ ) of 40 mm. The upper cavity had a cover depth of  $2D$ . The twin tunnels with an inclined arrangement had a lateral centre-to-centre spacing of  $1.5D$  and were offset vertically by  $1.5D$ . Nine linear variable differential transformers (LVDTs) were placed symmetrically above the model with a uniform spacing of 45 mm.

The procedures for the preparation of the centrifuge model test were as follows:

- Consolidating the slurry: Speswhite kaolin slurry with a water content of 120% was prepared first. A pressure of 500 kPa was applied on the sample to achieve full consolidation (cf. Fig. 14a).

- Unloading the sample: The applied pressure was subsequently reduced to 250 kPa so that the sample was in an overconsolidated state (cf. Fig. 14b).
- Installing the tunnels: After the consolidation pressure was completely removed from the sample, the exposed clay surface was quickly sealed with silicon oil to prevent the evaporation of pore water. Then, two tunnel cavities were bored at the positions of the twin tunnels (cf. Fig. 14c).
- Acceleration model: Both cavities were supported by water within a latex membrane. Once the above-mentioned work was performed, the assembled model was placed on the centrifuge swing. The model was accelerated to 100 g within 4 min and left running for 24 h. The preparation of the twin tunnel centrifuge model was complete when the equilibrium state was reached (cf. Fig. 14d).

The modelling of twin tunnel construction can be divided into the following four steps in the centrifuge model test:

- 1st tunnelling event* The 1st tunnel was excavated within 60 s. A certain volume of water was removed from the 1st tunnel cavity via the fluid control system

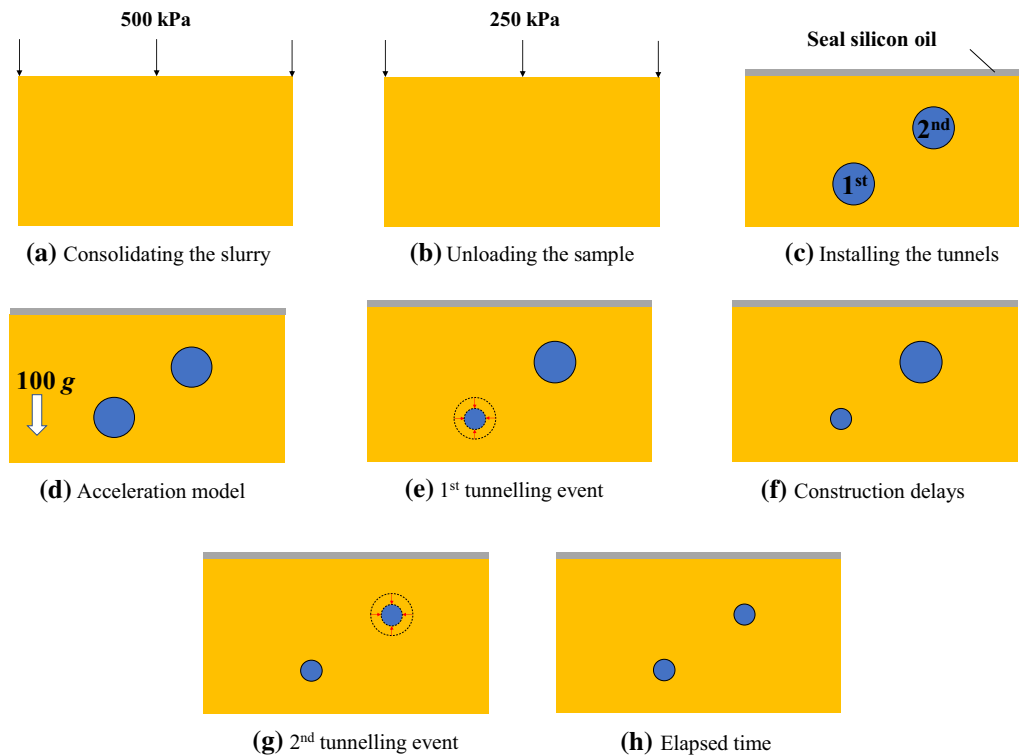


**Fig. 14** Test procedure

to simulate the first tunnelling event, which led to a volume loss of 3% (cf. Fig. 14e).

- b. *Construction delays* A time interval of 180 s was set immediately after the completion of the 1st tunnelling event and before the excavation of the 2nd tunnel. The time interval mimicked a practical construction delay of 3 weeks (cf. Fig. 14f).
- c. *2nd tunnelling event* The 2nd tunnel was excavated within 60 s. Similarly, the same amount of water was discharged from the 2nd tunnel cavity via the fluid control system (cf. Fig. 14g).
- d. *Elapsed time* After the completion of the twin-tunnelling event, the centrifuge was run for at least an hour after the test to model long-term soil settlement (cf. Fig. 14h).

## Numerical simulation

The process of centrifuge model testing was carefully reproduced by the following simulation procedure:

- a) *Initial state ( $K_0$  consolidation)* An effective vertical stress of 500 kPa was applied to the model. The stress condition of  $K_0 = 1 - \sin \phi'$  was adopted in equilibrium with an applied surcharge of 500 kPa. During the soil-making process in step (a) to step (b),

drainage was allowed at both the top and bottom of this model (cf. Fig. 15a).

- b) *One-dimensional swelling* The surcharge was reduced to 250 kPa, while the pore pressure of the model was maintained at zero, corresponding to a completely consolidated state (cf. Fig. 15b).
- c) *Installation of the tunnels* Drainage was not allowed at this step. At the very beginning of this step, the surcharge was deactivated. Two tunnel cavities were subsequently installed by removing the corresponding elements. In addition, a pore pressure of  $-250$  kPa was imposed on the soil model to maintain the effective stress of 250 kPa, which was the same as the one at the end of the previous step (cf. Fig. 15c).
- d) *Consolidation in flight* The removed cavity elements were replaced with elastic ‘water’ elements. The water element had a density of  $1000 \text{ kg/m}^3$ , bulk modulus  $K_w$  of 2180 MPa and a tiny shear modulus  $G_w$ . From this step, the bottom of the model was set to be completely permeable. To simulate the true initial stress state, the gravitational force was then increased to 100 g in 4 min, followed by a sufficiently long duration of constant loading for full consolidation (cf. Fig. 15d).

The process of constructing twin tunnels is described below:

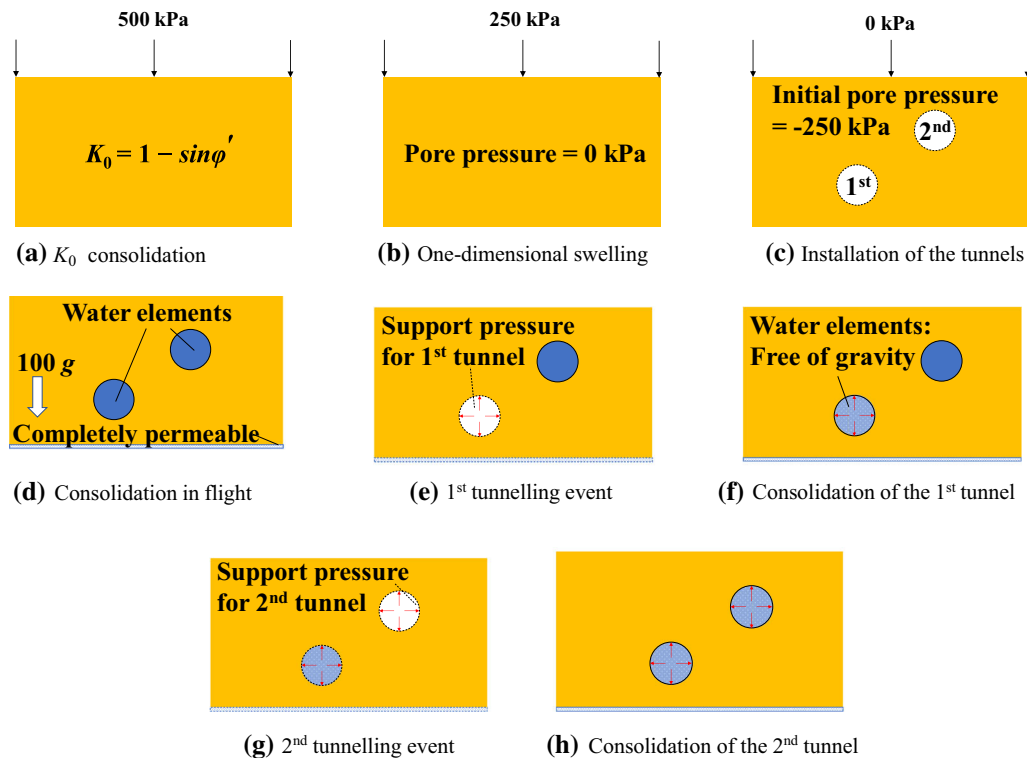


**Fig. 15** Simulation procedure

- (a) *1st tunnelling event* Water elements were removed at the very beginning of this step, and a relatively low pressure was imposed on the cavity surface to achieve a volume loss of 3% in 60 s (cf. Fig. 15e).
- (b) *Consolidation of the 1st tunnel* Water elements were reactivated but were free from gravity. A 180-s interval was set as a time delay after the 1st tunnelling event (cf. Fig. 15(f)).
- (c) *2nd tunnelling event* The operations performed in step (a) for the 1st tunnel were repeated for the 2nd tunnel (cf. Fig. 15g).
- (d) *Consolidation of the 2nd tunnel:* The operations performed in step (b) for the 1st tunnel were repeated for the 2nd tunnel (cf. Fig. 15h).

**Supplementary Information** The online version contains supplementary material available at <https://doi.org/10.1007/s11440-022-01541-5>.

**Acknowledgements** The authors would like to acknowledge the financial support from the National Natural Science Foundation of China (Grant No. 51808387).

## References

1. Addenbrooke TI, Potts DM (2001) Twin tunnel interaction: surface and subsurface effects. *Int J Geomech* 1:249–271
2. Chapman DN, Ahn SK, Hunt DV (2007) Investigating ground movements caused by the construction of multiple tunnels in soft ground using laboratory model tests. *Can Geotech J* 44:631–643
3. Chehade FH, Shahrour I (2008) Numerical analysis of the interaction between twin-tunnels: influence of the relative position and construction procedure. *Tunn Undergr Space Technol* 23:210–214
4. Chen RP, Li J, Kong LG, Tang LJ (2013) Experimental study on face instability of shield tunnel in sand. *Tunn Undergr Space Technol* 33:12–21
5. Chen S-L, Li G-W, Gui M-W (2009) Effects of overburden, rock strength and pillar width on the safety of a three-parallel-hole tunnel. *J Zhejiang Univ-Sci A* 10:1581–1588
6. Chu B-L, Hsu S-C, Chang Y-L, Lin Y-S (2007) Mechanical behavior of a twin-tunnel in multi-layered formations. *Tunn Undergr Space Technol* 22:351–362
7. Clough GW, Schmidt B (1981) Design and performance of excavations and tunnels in soft clay. *Develop Geotech Eng* 20:567–634
8. Cooper ML, Chapman DN, Rogers CDF, Chan AHC (2002) Movements in the piccadilly line tunnels due to the heathrow express construction. *Geotechnique* 52:243–257
9. Cording, E.J., 1975. Displacement around soft ground tunnels, general report: session IV, Tunnels in soil. In: Proc. of 5th Panamerican congress on SMFE
10. Divall S (2013) Ground movements associated with twin-tunnel construction in clay. City University London, London
11. Divall, S., Goodey, R., 2012. Novel apparatus for generating ground movements around sequential twin tunnels in over-consolidated clay. In: Online publication by Proceedings of the ICE-geotechnical engineering, pp 10–11
12. Divall S, Goodey RJ (2015) Twin-tunnelling-induced ground movements in clay. *Proc Inst Civ Eng-Geotech Eng* 168:247–256

13. Divall S, Goodey R, Stallebrass S (2017) Twin-tunnelling-induced changes to clay stiffness. *Géotechnique* 67:906–913
14. He C, Feng K, Fang Y, Jiang Y-C (2012) Surface settlement caused by twin-parallel shield tunnelling in sandy cobble strata. *J Zhejiang Univ Sci A* 13:858–869
15. Hunt D (2005) Predicting the ground movements above twin tunnels constructed in London Clay. University of Birmingham, Birmingham
16. Idinger G, Aklik P, Wu W, Borja R (2011) Centrifuge model test on the face stability of shallow tunnel. *Acta Geotech* 6:105–117
17. Kim S, Burd H, Milligan GE (1996) Interaction between closely spaced tunnels in clay. *Geotechnical aspects of underground construction in soft ground*, pp 543–548
18. Kim S, Burd H, Milligan G (1998) Model testing of closely spaced tunnels in clay. *Geotechnique* 48:375–388
19. Kirsch A (2010) Experimental investigation of the face stability of shallow tunnels in sand. *Acta Geotech* 5:43–62
20. Liu W, Zhao Y, Shi P (2018) Face stability analysis of shield driven tunnels shallowly buried in dry sand using 1 g large-scale model tests. *Acta Geotech* 13:693–705
21. Ma SK, Duan ZB, Huang Z (2022) Study on the stability of shield tunnel face in clay and clay-gravel stratum through large-scale physical model tests with transparent soil. *Tunn Undergr Space Technol* 119:104199
22. Mair RJ (1978) Centrifugal modelling of tunnel construction in soft clay
23. Mašín D (2004) Laboratory and numerical modelling of natural clays. MPhil-Thesis, City University, London
24. O'Reilly MP, New BM (1982) Settlements above tunnels in the United Kingdom—their magnitude and prediction. *Tunnelling* 82. The Institution of Mining and Metallurgy, London, pp 55–64
25. O'reilly MP, New B (1982) Settlements above tunnels in the United Kingdom—their magnitude and prediction
26. Peck RB (1969) Deep excavations and tunneling in soft ground. In: *Proc. 7th ICSMFE*, 1969, pp 225–290
27. Rankin W (1988) Ground movements resulting from urban tunnelling: predictions and effects. *Geol Soc Lond Eng Geol Spec Publ* 5:79–92
28. Stallebrass S (1990) The effect of recent stress history on the deformation of overconsolidated soils. PhD thesis. City University London, UK
29. Stallebrass S, Taylor R (1997) The development and evaluation of a constitutive model for the prediction of ground movements in overconsolidated clay. *Géotechnique* 47:235–253
30. Suwansawat S, Einstein HH (2007) Describing settlement troughs over twin tunnels using a superposition technique. *J Geotech Geoenviron Eng* 133:445–468
31. Viggiani G (1992) Small strain shear stiffness of fine grained soils. PhD Thesis, City Univ. London
32. Yamaguchi I, Yamazaki I, Kiritani Y (1998) Study of ground-tunnel interactions of four shield tunnels driven in close proximity, in relation to design and construction of parallel shield tunnels. *Tunn Undergr Space Technol* 13:289–304
33. Zhang T, Taylor RN, Divall S, Zheng G, Sun J, Stallebrass SE, Goodey RJ (2019) Explanation for twin tunnelling-induced surface settlements by changes in soil stiffness on account of stress history. *Tunn Undergr Space Technol* 85:160–169
34. Zheng G, Zhang T, Diao Y (2015) Mechanism and countermeasures of preceding tunnel distortion induced by succeeding EPBS tunnelling in close proximity. *Comput Geotech* 66:53–65

**Publisher's Note** Springer Nature remains neutral with regard to jurisdictional claims in published maps and institutional affiliations.